Int J Adv Manuf Technol (2018) 94:4011–4021
DOI 10.1007/s00170-017-1120-5

ORIGINAL ARTICLE

Theoretical analysis and numerical simulation on the process mechanism of two-roller straightening

Gaochao Yu [1,2] · **Ruixue Zhai** [1,2] · **Jun Zhao** [1,2] · **Rui Ma** [1,2]

Received: 24 May 2017 / Accepted: 13 September 2017 / Published online: 27 September 2017

Abstract The two-roller straightening process has an irreplaceable position in the finishing process of metal bars. In this paper, the deformation of bar is macroscopically recognized by analyzing the deformation path in the roller gap. Graphic method and mathematical induction are adopted to analyze the deformation process of the section of bar. The equation of residual curvature and the unified equation of residual curvature are established. It is proved that although the initial curvature of each section of bar is different, the difference of initial curvature is eliminated by the reciprocating bending, and the process mechanism of the two-roller straightening is revealed. The speed of curvature unification is determined mainly by the ratio of plastic modulus to elastic modulus. The greater the ratio of plastic modulus to elastic modulus is, the slower the speed of curvature uniformity is, and the more the bending time required. Then, the quantitative analysis model and finite element model of the two-roller straightening process are established by taking the three-section constant curvature roller gap model as an example. The stress, strain, and straightness are discussed, and the variation of the elastic area ratio, the residual curvature, and the residual deflection with the bending time is quantitatively analyzed. The results verify the process mechanism of the two-roller straightening, and the design principle of roller shape is given.

Keywords Two-roller straightening · Process mechanism · Graphic method · Mathematical induction · Numerical simulation

✉ Ruixue Zhai
zhairuixue@ysu.edu.cn

Gaochao Yu
gch_yu@ysu.edu.cn

Jun Zhao
zhaojun@ysu.edu.cn

Rui Ma
mar@ysu.edu.cn

[1] Key Laboratory of Advanced Forging & Stamping Technology and Science (Yanshan University), Ministry of Education of China, Qinhuangdao, People's Republic of China

[2] College of Mechanical Engineering, Yanshan University, No.438, Hebei Street, 066004, Qinhuangdao, Haigang District, People's Republic of China

1 Introduction

Two-roller straightening process has many advantages, such as all-direction straightening, high precision, good surface quality, and simple equipment, which has an irreplaceable position in the finishing process of metal bars [1]. However, in the aspect of roller shape design and process parameters determination, the theory is still not mature, and the operator mainly relies on experience, which leads to poor straightening accuracy and low straightening efficiency. The reason is that the theoretical foundation and the experience accumulation are insufficient. Therefore, it is necessary to deeply understand the process mechanism of the two-roller straightening.

The multi-roller straightening [2–4] and multi-point bending one-off straightening [5] can not straighten all directionally on the pipe or bar with circular section, so the two-roller straightening process emerges as the times require. In the initial stage of study, the scholars mainly analyzed the two-roller straightening process based on the elastic-plastic theory, in which a large amount of simplification is carried out, such as material constitutive model, stress state, and contact condition. Talukder et al. [6–9] analyzed the main factors

of different types of skew roller straightening process, such as moment, straightness, straightening speed, and straightening force, gave the advantages and disadvantages and limitations of different types of skew roller straightening process, and optimized the arrangement of the straightening roller. According to the two-roller straightening method, Kawai et al. [10] developed a three-roller straightening process for straightening the seamless aluminum tubes. The influence of the roller angle and the guide angle and the length of the straightening roller on the straightness were discussed. Li et al. [11] adopted the envelope theory to propose a convenient and universal method for determining the roller shape of skew roller. Cui [1] analyzed systematically the two-roller straightening process, and gave the determination method of structural parameters, force and energy parameters, and process parameters. Based on the classical elastoplastic theory, Wu et al. [12] analyzed the bending deformation of bar, considered that the two-roller straightening process is a process of alternating bending and reverse bending, and used iterative method to study the curvature convergence in the two-roller straightening process.

At the end of the twentieth century, the numerical simulation method was applied to the complex-forming problem. With the help of numerical simulation, the researchers have got a better and deeper understanding on the two-roller straightening process. In order to realize the straightening of thin-walled aluminum tubes, Huh et al. [13] established the finite element model of skew roller straightening, carried out the analysis with the fractional model and Taguchi method for evaluation of the effect of process parameters. The optimum combination of process parameters is determined. Kuboki et al. [14] established four explicit and implicit finite element models on the skew roller straightening process, and found an optimal finite element model by comparing the simulation results. Mutrux et al. [15] used a modified Chaboche material constitutive model to simulate the two-roller straightening process accurately, and predicted the cyclic softening and residual stress distribution. Wang et al. [16, 17] analyzed the two-roller straightening process by finite element simulation and physical experiment, optimized two parameters of the roller gap and guide plate spacing, which reduced the adjustment time of the roller gap and the replacement frequency of the guide plate. Moon et al. [18] studied the residual stress and dimensional change of bars during the two-roller straightening process by finite element method, and the results show that the roller spacing has obvious influence on both and the roller angle has no obvious influence on both. Ma et al. [19] studied the neutral layer offset of bar in two-roll straightening process, and established a model, which provides a reference to further study the straightening mechanism. Jindřich et al. [20] used Euler algorithm to describe the longitudinal material flow, and used the classical Lagrangian approach to describe the transversal deformation in the finite element simulation on the skew roller straightening. It is expected to realize the on-line prediction and control of the straightening process parameters. Zhang et al. [21–23] established the mathematical model of the straightening curvature-radius on thin-walled tubes by using the elastic-plastic theory and classic unloading rule and a prediction model of section flattening by using the minimum energy method, but the latter needs to be further verified and improved. Wang et al. [24] proposed a theoretical analysis method, and simulated the skew roller straightening process of the bar. The results show that the curve of curvature and deflection is sinusoidal, and the residual stress is a spiral distribution.

In order to explain the process mechanism of the two-roller straightening, the deformation of bar is recognized macroscopically by analyzing the deformation path in the roller gap. Graphic method and mathematical induction are adopted to analyze the deformation process of the section of bar. Then, the quantitative analysis model and finite element model of the two-roller straightening process are established by taking the three-section constant curvature roller gap model as an example. The stress, strain, and straightness are discussed, and the variation of the elastic area ratio, the residual curvature, and the residual deflection with the bending time is quantitatively analyzed.

2 Two-roller straightening process

The main work parts of the two-roller straightening device are composed of a convex roller and a concave roller, and the two rollers are inclined in an angle to rotate at the same direction, as shown in Fig. 1. In order to achieve continuous and all-directional straightening, the circular bar rotates and moves through the gap between the convex roller and the concave roller under the action of rollers. As a result of the roller gap slightly larger than the outer diameter of the circular bar, the stress state of the circular bar can be approximated to pure bending [15].

3 Process mechanism analysis

3.1 Deformation path

As shown in Fig. 2, the plastic deformation is produced in a certain range of the bar by pressing from the rollers. The plastic deformation zone is mainly determined by roller shape, roller gap, roller angle, and material properties of the bar. Without losing generality, a particle A on the surface of the bar is taken. The spatial trajectory of particle A is a spiral line centered on the bar axis. All the zones outside the plastic deformation zone have no effect on straightening, where the deformation of particle A is full elastic. When the particle A

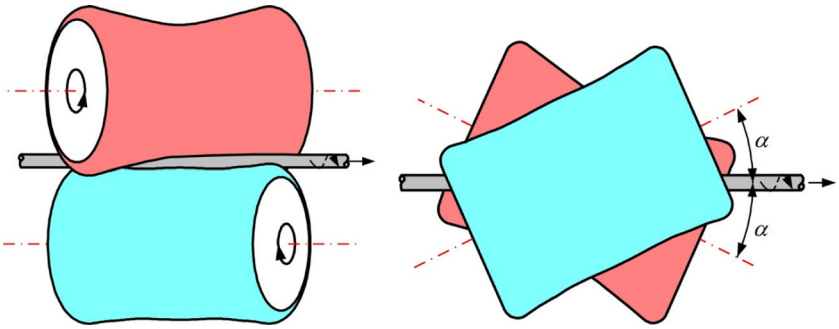

Fig. 1 The schematic diagram of two-roller straightening

(a) Main view (b) Lower view

enters the plastic deformation zone, the section where the particle A locates undergoes several times of elastic-plastic bending deformation.

In Fig. 2, the section where the particle A locates undergoes a total of 11 plastic bending. In each plastic bending deformation, the maximum deformation of particle A occurs at position 1, position 2, ..., and position 11, respectively. It is difined that if the particle A undergoes compression deformation, it is a positive bending, and if the particle A has a tensile deformation, it is a reverse bending. Therefore, in position 1, position 3, position 5, position 7, position 9, and position 11, the section experiences positive bending, and reverse bending occurs at position 2, position 4, position 6, position 8, and position 10. The bending curvature of each position is shown in Table 1. The value of positive curvature is positive, while the value of reverse curvature is negative. So K_1, K_3, and K_5 are positive, and K_2, K_4, and K_6 are negative. The order of the section undergoes multiple bending is $K_1 \rightarrow K_2 \rightarrow K_3 \rightarrow K_4 \rightarrow K_5 \rightarrow K_6 \rightarrow K_5 \rightarrow K_4 \rightarrow K_3 \rightarrow K_2 \rightarrow K_1$.

Position	1 and 11	2 and 10	3 and 9	4 and 8	5 and 7	6
Curvature	K_1	K_2	K_3	K_4	K_5	K_6

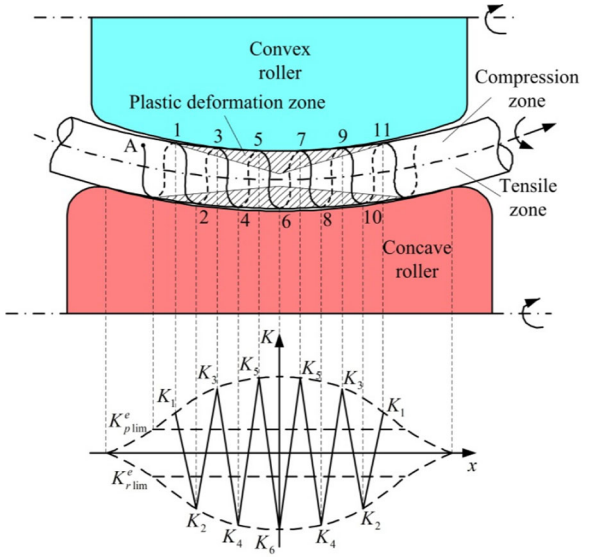

Fig. 2 Deformation path of particle

3.2 Graphic analysis

Three representative sections of A, B, and C are taken from the bar, and their initial curvature are K_{A0}, K_{B0}, and K_{C0}, respectively. The section A is at the extreme point of the transition from the positive curvature to the negative curvature of the bar, and its curvature value is zero, $K_{A0} = 0$. Section B is in the positive curvature part of the bar, and its curvature value is positive, $K_{B0} > 0$. Section C is in the negative curvature part of the bar, and its curvature value is negative, $K_{C0} < 0$.

The functional relation between the moment and curvature of three sections is expressed as

$$M_A = \int_A \sigma w dA = \int_A f[(K - K_{A0})\, w] w dA \quad (1)$$

$$M_B = \int_A \sigma w dA = \int_A f[(K - K_{B0})\, w] w dA \quad (2)$$

$$M_C = \int_A \sigma w dA = \int_A f[(K - K_{C0})\, w] w dA \quad (3)$$

where σ is stress, w is radial coordinate value, A is integral area, and M_A, M_B, and M_C are the moment of section A, B, and C, respectively.

From the Eqs.(1)–(3), it can be seen that the functions of the moment and curvature are the same under the condition of uniform material, but the moment moves in different degrees because of the difference of initial curvatures of three sections. Therefore, graphic method is used to analyze the curvature change of three sections in the two-roller straightening process.

In order to make the graphic analysis universal, the effects of deformation strengthening, Baushinger effect and cyclic softening in the reciprocating bending process are taken into account, and the discussion is divided into 3 cases:

Table 1 Bending curvature of each position

Position	1 and 11	2 and 10	3 and 9	4 and 8	5 and 7	6
Curvature	K_1	K_2	K_3	K_4	K_5	K_6

(1) Case 1: considering deformation strengthening without considering Baushinger effect and cyclic softening. The positive elastic limit moment and the reverse elastic limit moment are equal.

$$\left|M_{\mathrm{lim}}^{\mathrm{p}}\right| = \left|M_{\mathrm{lim}}^{\mathrm{r}}\right| \tag{4}$$

The change process of the curvatures of three sections after springback in case 1 is shown in Fig. 3.

(2) Case 2: considering deformation strengthening and Baushinger effect without considering cyclic softening. The positive elastic limit moment is greater than the reverse elastic limit moment.

$$\left|M_{\mathrm{lim}}^{\mathrm{p}}\right| > \left|M_{\mathrm{lim}}^{\mathrm{r}}\right| \tag{5}$$

The change process of the curvatures of three sections after springback in case 2 is shown in Fig. 4.

(3) Case 3: considering deformation strengthening, Baushinger effect and cyclic softening. According to the cyclic stress-stain hysteresis curves obtained from tension-compression test [15], it is seen that the macro mechanical properties of the materials gradually stabilized with the increase of cycle time. In this analysis, it is

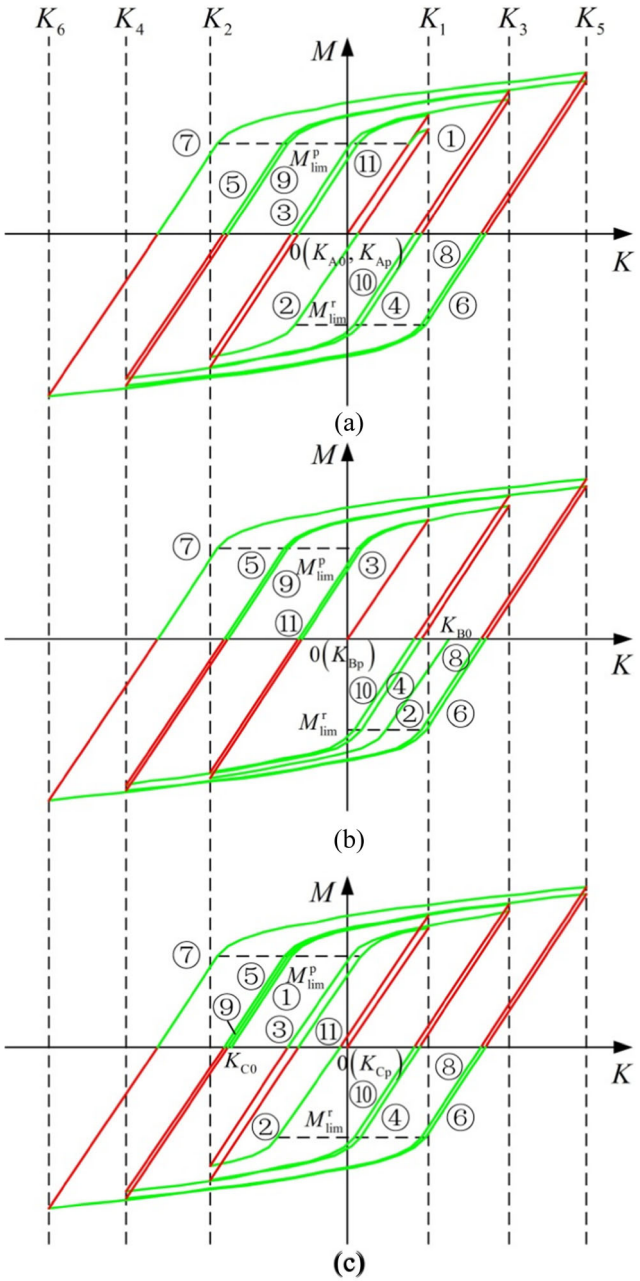

Fig. 3 The deformation process of cross section considering deformation strengthening without considering Baushinger effect and cyclic softening

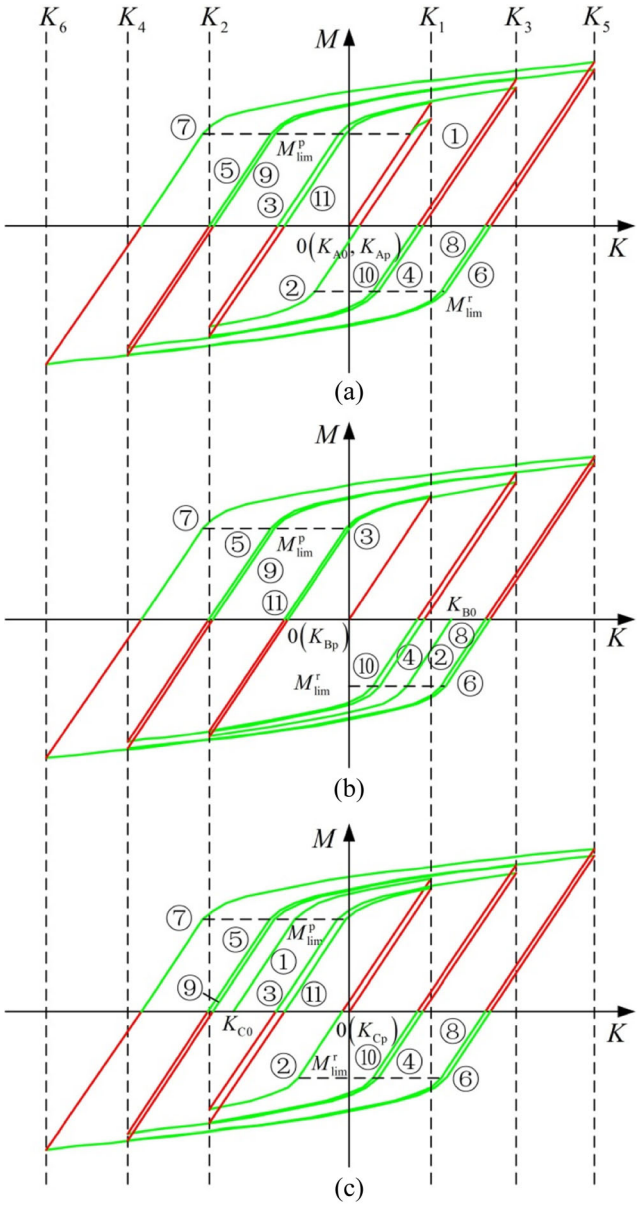

Fig. 4 The deformation process of cross section considering deformation strengthening and Bashinger effect without considering cyclic softening

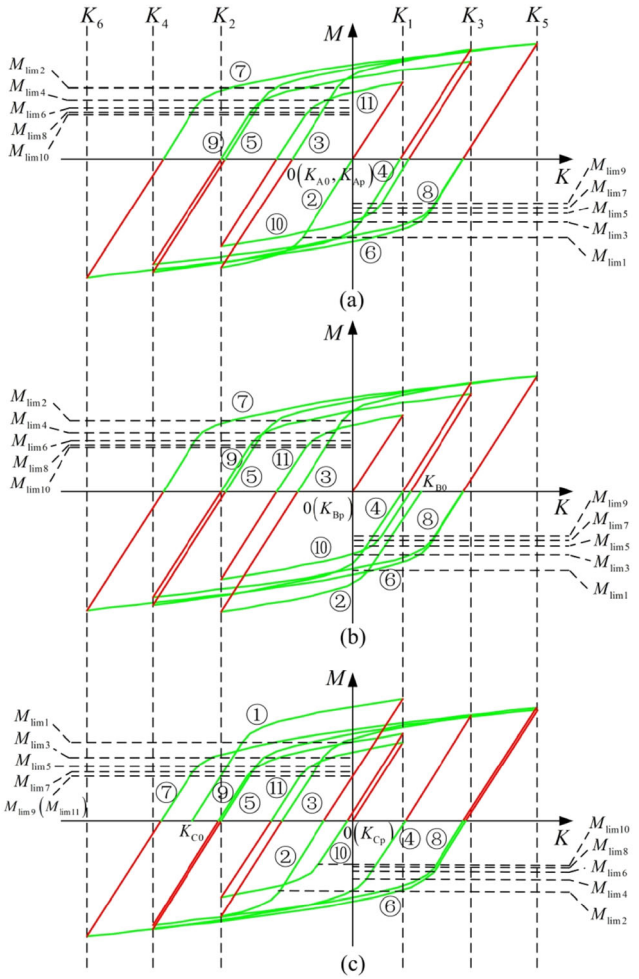

Fig. 5 The deformation process of cross section considering deformation strengthening Bashinger effect and cyclic softening

considered that the mechanical properties are stable when the number of bending time reaches 10 times.

$$|M_{\lim 1}| > |M_{\lim 2}| \tag{6}$$

$$|M_{\lim 1}| > |M_{\lim 3}| > |M_{\lim 5}| > |M_{\lim 7}| > |M_{\lim 9}| = |M_{\lim 11}| = \ldots = \left|M_{\lim(2n-1)}\right|, n \geq 1 \tag{7}$$

$$|M_{\lim 2}| > |M_{\lim 4}| > |M_{\lim 6}| > |M_{\lim 8}| > |M_{\lim 10}| = |M_{\lim 12}| = \ldots = \left|M_{\lim(2n)}\right|, n \geq 1 \tag{8}$$

where $M_{\lim(n)}$ is the elastic limit moment at the n bending.

The change process of the curvatures of three sections after springback in case 3 is shown in Fig. 5.

In the moment-curvature coordinate system, the positions of the initial curvatures of three sections are located in the origin, the positive axis of the curvature axis and the negative axis of the curvature axis, respectively. As shown in Figs. 3, 4, and 5, it is seen that the three sections undergo 11 bending and reverse bending processes in turn, the residual curvatures of three sections incuding, K_{Ap}, K_{Bp}, and K_{Cp}, gradually approach to the origin of the coordinate system, and their value become zero. Therefore, it is proved that although the initial curvature of each section is different, the difference can be eliminated by undergoing the same bending and reverse bending loading path, and if a set of proper bending curvature is set, the residual curvature of each section of the bar can be uniformly zero, that is, the aim of straightening is achieved.

3.3 Elastic-plastic analysis

Above, the two-roller straightening process is revealed visually by the graphic method. In this section, the mathematical induction method and the linear simple kinematic hardening (LSKH) model [25] are used to further investigate the variation of residual curvature in the two-roller straightening process.

3.3.1 Analysis object

Without loss of generality, the circular pipe is used as the object of analysis. The outer diameter of the pipe is R_1 and the inner diameter is R_2. When $R_2 = 0$, the circular pipe can become to a circular bar, as shown in Fig. 6. The center of the circle at any section is used as the origin o, the normal direction of the axis is w coordinate axis, and the tangent direction is v coordinate axis, so the coordinate system $ouvw$ is established. In this coordinate system, the v axis passes through the centers of all sections and is perpendicular to all sections.

3.3.2 Constitutive model

Since the elastic-plastic boundary point is considered in the analysis process, the moment expression of the circular pipe is more complicated than that of rectangular section [26], which is very unfortunate for the derivation of the residual curvature of reciprocating bending. Therefore, the linear simple kinematic hardening constitutive model is simplified, as shown

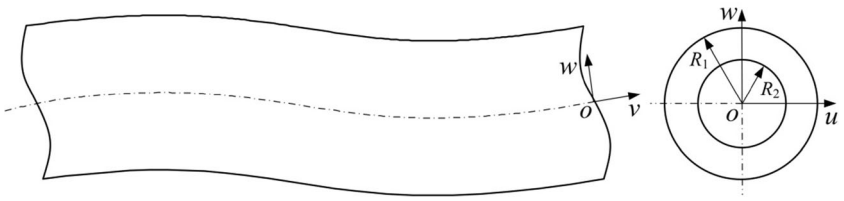

Fig. 6 Geometry diagram of round pipe

$$\sigma = \begin{cases} D\varepsilon + \sigma_0 & \varepsilon > 0 \\ D\varepsilon - \sigma_0 & \varepsilon < 0 \end{cases}$$

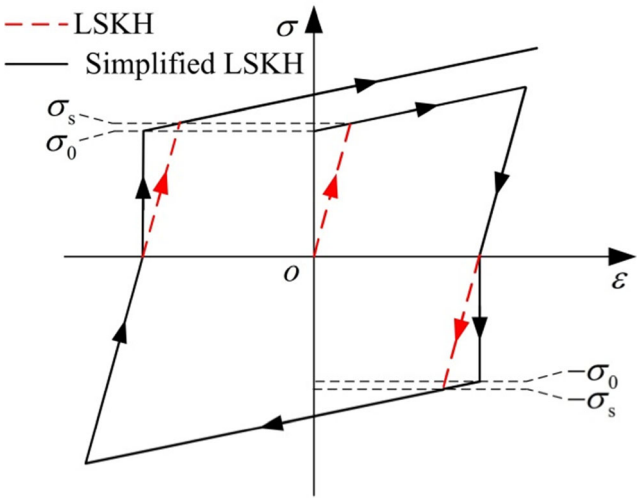

Fig. 7 Simplified linear simple kinematic hardening constitutive model

in Fig. 7. In the simplified linear simple kinematic hardening constitutive model, it is considered that the whole section is in a state of full plastic deformation, and the elastic modulus, yield stress, and plastic modulus do not change with the number of loading. The mathematical expression is as follows

$$\sigma = \begin{cases} D\varepsilon + \sigma_0 & \varepsilon > 0 \\ D\varepsilon - \sigma_0 & \varepsilon < 0 \end{cases} \tag{9}$$

3.3.3 Mathematical induction

Since the deformation of each section of the bar in the two-roller straightening process is continuous, the curvature after springback of the former bending is considered as the initial curvature of the current bending. According to the springback equation of small curvature plane bending [27], the recurrence formula of reciprocating bending is as follows

$$K_{pn} = \begin{cases} K_n - \dfrac{M_n(K_n,\ K_0)}{EI} & n = 1 \\ K_n - \dfrac{M_n\left(K_n,\ K_{p(n-1)}\right)}{EI} & n \geq 2 \end{cases} \tag{10}$$

Table 3 Roller shape design parameters

Straightening diameter /mm	Straightening speed /m min^{-1}	Roller angle α/°
30 ~ 50	30	20 ~ 25

The functional relation between the moment and bending curvature in unit length can be expressed as

$$M = \int_{-R_1}^{R_1} \sigma w dw = \begin{cases} DI_u(K - K_0) + M_0 & K \geq K_0 \\ DI_u(K - K_0) - M_0 & K < K_0 \end{cases} \tag{11}$$

where $M_0 = \frac{4\left(R_1^3 - R_2^3\right)\sigma_0}{3}$ and $I_u = \frac{\pi\left(R_1^4 - R_2^4\right)}{4}$.

By using the mathematical induction, when the first bending is reversed, the residual curvature equation of the n-th bending can be expressed as

$$K_{pn} = K_n - \frac{D}{E}(K_n - K_{n-1}) - \left(\frac{D}{E}\right)^2 (K_{n-1} - K_{n-2}) - \ldots - \left(\frac{D}{E}\right)^n (K_1 - K_0) + (-1)^{n+1} \frac{16\left(R_1^3 - R_2^3\right)\sigma_0\left[1 - \left(-\frac{D}{E}\right)^n\right]}{3\pi\left(R_1^4 - R_2^4\right)(E + D)} \tag{12}$$

When the first bending is positive, the residual curvature equation is

$$K_{pn} = K_n - \frac{D}{E}(K_n - K_{n-1}) - \left(\frac{D}{E}\right)^2 (K_{n-1} - K_{n-2}) - \ldots - \left(\frac{D}{E}\right)^n (K_1 - K_0) + (-1)^n \frac{16\left(R_1^3 - R_2^3\right)\sigma_0\left[1 - \left(-\frac{D}{E}\right)^n\right]}{3\pi\left(R_1^4 - R_2^4\right)(E + D)} \tag{13}$$

Because $\frac{D}{E} \leq 1$, when the bending times n is large enough, in Eq.(12) and Eq. (13) n-th terms on the $\frac{D}{E}$ can be ignored, when the first bending is reversed, the unified equation of residual curvature is

$$\overline{K}_{pn} = K_n - \frac{D}{E}(K_n - K_{n-1}) - \left(\frac{D}{E}\right)^2 (K_{n-1} - K_{n-2}) - \ldots - \left(\frac{D}{E}\right)^{n-1} (K_2 - K_1) + (-1)^{n+1} \frac{16\left(R_1^3 - R_2^3\right)\sigma_0}{3\pi\left(R_1^4 - R_2^4\right)(E + D)} \tag{14}$$

Table 2 Material properties of the bar

Yield stress σ_s/MPa	Elastic modulus E/MPa	Plastic modulus D/MPa	Elongation δ/%	Poisson ratio ν	Density ρ/(kg m^{-3})
900	206,000	1730	12	0.3	7.83×10^3

Table 4 Bending curvature of each bending

Bending times n	1	2	3	4	5	6	7	8
Bending curvature $K/(10^{-4}\ \mathrm{mm}^{-1})$	4.17	−4.17	4.17	−4.17	4.85	−4.85	14.6	−14.6
Bending times n	9	10	11	12	13	14	15	16
Bending curvature $K/(10^{-4}\ \mathrm{mm}^{-1})$	14.6	− 14.6	4.85	− 4.85	4.17	− 4.17	4.17	− 4.17

And when the first bending is positive, the unified equation of residual curvature is

$$\overline{K}_{pn} = K_n - \frac{D}{E}(K_n - K_{n-1}) - \left(\frac{D}{E}\right)^2 (K_{n-1} - K_{n-2}) - \ldots - \left(\frac{D}{E}\right)^{n-1} (K_2 - K_1) + (-1)^n \frac{16\left(R_1^3 - R_2^3\right)\sigma_0}{3\pi\left(R_1^4 - R_2^4\right)(E + D)} \quad (15)$$

Eqs. (14) and (15) can be expressed as

$$\overline{K}_{pn} = f(D,\ E,\ \sigma_0,\ R_1,\ R_2,\ K_1,\ K_2,\ \ldots,\ K_n) \quad (16)$$

It is proved from Eq. (16) that the difference of initial curvature of the section is eliminated by reciprocating bending, and finally the different curvatures are unified to the same direction and the same value. According to Eqs. (14) and (15), when the mechanical properties and geometrical parameters are defined, the residual curvature of each section of the bar can be united to zero by choosing a suitable set of bending curvature. The speed of curvature unification is determined mainly by the ratio of plastic modulus to elastic modulus. The greater the ratio of plastic modulus to elastic modulus is, the slower the speed of curvature uniformity is, and the more the bending time required, i.e., the more the number of spiral leads is.

4 Quantitative analysis

4.1 Initial conditions

The bar with length of 1000 mm and diameter of 30 mm is chosen as the analytical object. The material properties are shown in Table 2.

Three-section constant curvature roller gap model proposed by Cui [1] is selected. The design parameters of the roller shape are shown in Table 3. The straightening roller is divided into three sections: waist section, abdomen section, and chest section. The working length of the straightening roller is designed with 8 spiral leads. Since each section of the bar is bent once through half a spiral lead, each section undergoes 16 bends. According to the curvature design of the roller, the curvature of each section is shown in Table 4, and the variation of curvature with bending time is shown in Fig. 8.

In order to make quantitative analysis without loss of generality, 5 micro-beams [26] with different initial curvatures, including 3×10^{-4} mm^{-1}, 1.5×10^{-4} mm^{-1}, 0 mm^{-1}, -1.5×10^{-4} mm^{-1}, and -3×10^{-4} mm^{-1}, are selected. The initial deflection of each micro-beams can be obtained by Eq. (17), which are 37.7 mm/m, 18.8 mm/m, 0 mm/m, − 18.8 mm/m, and − 37.7 mm/m.

$$K = \frac{2v}{500^2 + v^2} \quad (17)$$

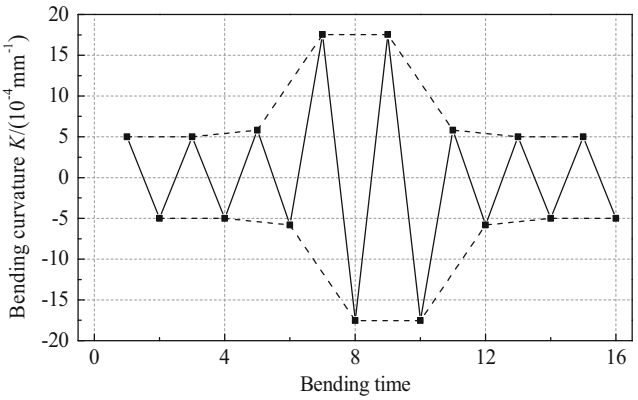

Fig. 8 Variation of bending curvature with bending time

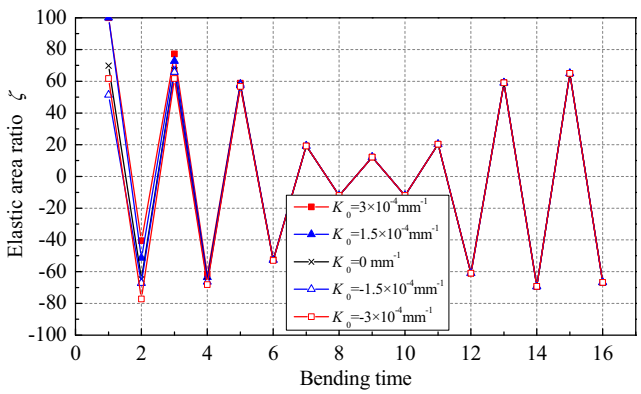

Fig. 9 Variation of elastic area ratio with bending times

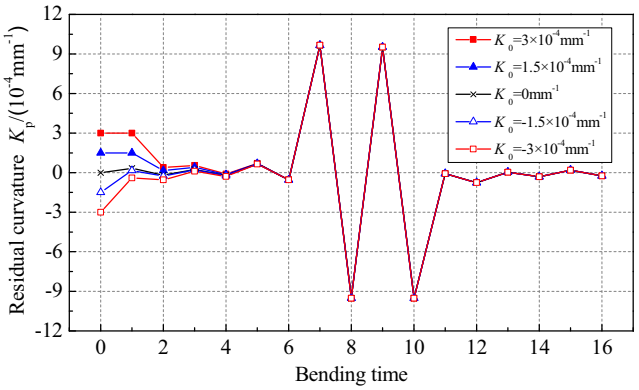

Fig. 10 Variation of residual curvature with bending times

4.2 Moment equation

When $|\varepsilon_{\max}| \le \frac{\sigma_s}{E}$, the section of the bar is in full elastic state, and the elastic limit curvature of positive bending and reverse bending is respectively

$$K^{e}_{plim} = K_0 + \frac{\sigma_s}{R_1 E} \tag{18}$$

$$K^{e}_{rlim} = K_0 - \frac{\sigma_s}{R_1 E} \tag{19}$$

In order to improve the accuracy of quantitative analysis, the linear simple kinematic hardening constitutive model is adopted, and the functional relation between the moment and curvature in unit length can be expressed as

$$M = \int_{-R_1}^{R_1} \sigma w dw = \begin{cases} I_u D(K-K_0) + \frac{R_1^4}{2}\arcsin\frac{w_s}{R_1}(K-K_0)(E-D) + \frac{w_s R_1^2}{2}\sqrt{R_1^2-w_s^2}(K-K_0)(D-E) \\ +w_s^3\sqrt{R_1^2-w_s^2}(K-K_0)(E-D) + \frac{4\sigma_0}{3}\sqrt{\left(R_1^2-w_s^2\right)^3} & K > K^{e}_{\mathrm{Plim}} \\ EI_u(K-K_0) & K^{e}_{\mathrm{Rlim}} \le K \le K^{e}_{Plim} \\ I_u D(K-K_0) + \frac{R_1^4}{2}\arcsin\frac{w_s}{R_1}(K-K_0)(E-D) + \frac{w_s R_1^2}{2}\sqrt{R_1^2-w_s^2}(K-K_0)(D-E) \\ +w_s^3\sqrt{R_1^2-w_s^2}(K-K_0)(E-D) - \frac{4\sigma_0}{3}\sqrt{\left(R_1^2-w_s^2\right)^3} & K < K^{e}_{\mathrm{Rlim}} \end{cases} \tag{20}$$

$$w_s = \frac{\sigma_s}{E(K-K_0)} \tag{21}$$

$$\zeta = \frac{w_s}{R_1} \tag{22}$$

where ζ is the elastic area ratio.

4.3 Results and discussion

The geometrical parameters, material mechanical parameters, and bending curvature parameters are substituted into Eq. (10) and Eqs. (18)–(22), and the variation of the elastic area ratio, the residual curvature, and the residual deflection with the bending time can be obtained, as shown in Figs. 9, 10, and 11, respectively.

As can be seen from Fig. 9, the absolute value of the elastic area ratio decreases at first and then increases with the increase of the bending time. It shows that the deformation degree of the micro-beam increases first and then decreases, which conforms to the design principle of the roller shape and the basic principle of the two-roller straightening.

It can be seen from Figs. 10 and 11 that the variation of residual curvature and that of residual deflection with bending time both are basically the same, that is, the residual curvatures (residual deflections) of the 5 micro-beams with different initial curvatures (initial deflections) are approximately the same after 4 bends, and their values are close to zero. In the design of roller shape, the number of bending is 16, which is more than that of quantitative analysis. The reason is that in the quantitative analysis the material is assumed to be homogeneous, and the change of mechanical properties is not considered. What's more, considering the applicable range of the roller, as illustrated in Table 2, the smaller the diameter of the bar, the more the number of spiral lead, and the more the number of bending.

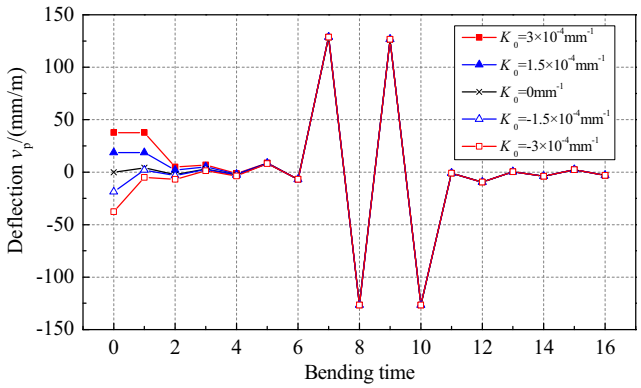

Fig. 11 Variation of residual deflection with bending times

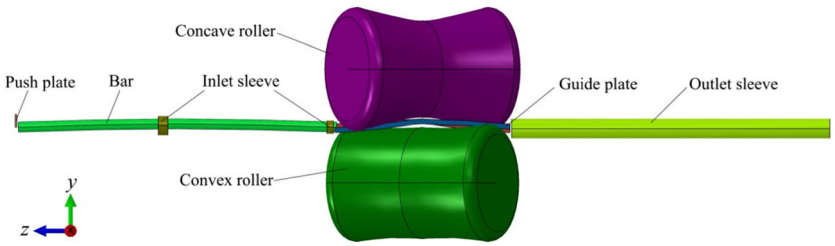

Fig. 12 Finite element model of two-roller straightening

5 Numerical simulation

5.1 Finite element model

The initial deflection curve of bar is assumed to be an equal curvature, and the deflection is 10 mm/m. According to the material parameters and the roller parameters in the quantitative analysis, the two-roller straightening process is simulated by ABAQUS 6.14, and the finite element model of two-roller straightening is shown in Fig. 12.

The main parts of the model include bar, convex roller, concave roller, guide plate, inlet sleeve, outlet sleeve, and push plate. The inlet sleeve is mainly used to restrict the swing of the bar in the straightening process, and the outlet sleeve is used for the recovery of the bar after straightening. The pushing plate provides an initial speed for the bar, so as to facilitate the bar to be inserted into the roller gap. The bar is set up as a deformable body, and the 8-node linear reduced integration element (C3D8R) is adopted, which is divided into 9200 elements. Other components are set as discrete rigid bodies. The surface-to-surface contact type is adopted, the penalty function is used for the tangential behavior, and the friction coefficient is 0.18. Because the two-roller straightening process is a very complicated nonlinear dynamic process, the ABAQUS/Explicit solver is used. The relevant process parameters are shown in Table 5.

5.2 Results and discussion

In order to study the change of stress and strain in straightening process, a cylindrical coordinate system (CSYS-1) is established by taking the center node of any section of the bar as the origin, and the coordinate system is converted to an absolute coordinate system. An outermost node, which is 415 mm from the entranceat, is taken as an example. The variation of axial stress, circumferential stress, and radial stress of the node with time in the straightening process is analyzed, as shown in Fig 13.

As illustrated in Fig. 13, during the bar through the roller gap, the node undergoes three stages: before entering the roller gap, in the roller gap, and after leaving the roller gap. In the straightening process, the value of the axial stress changes alternately, which shows that the node is subjected to a cyclic tensile-compressive load and the section is subjected to reciprocating bending. It proves the rationality of the mechanism analysis of the two-roller straightening. According to Saint Venant principle, when the node is out of the roller gap, it is affected by the local deformation of the bar, so the node still under alternating load before entering the gap and after leaving the gap. The axial stress of the node increases at first and then decreases, which is consistent with the design of the roller shape. When the straightening process is completed, the axial stress of the node is almost stable, and its value is about 250 MPa. Compared with the axial stress, the circumferential stress and radial stress are smaller, and the stress of the node is mainly determined by the axial stress.

In Fig. 13, the node undergod 8 cycles of tension-compression alternating load in the roller gap, which is consistent with the 8 spiral leads of the roller. It shows that the bar and the rollers are in good contact, and there is no slippage.

In order to show the alternation of axial tensile stress and compressive stress visually, the two node of A and B in the same section with central symmetry are taken as the analysis object. When the section is in the waist section of the roller, the variation law of the axial stress of the two nodes is analyzed during the section rotates for a week, as shown in Fig. 14.

As shown in Fig. 14, when the section is in the initial position (a), the node A has the maximum axial tensile stress, and the nodal B has the maximum axial compressive stress. As the section rotates from position (a) to position (c), the axial tensile stress of the node A decreases. When the section rotates 90 degrees and passes through the position (c), the tensile stress of the node A changes to compressive stress and increases gradually. Similarly, the axial compressive stress of the node B decreases gradually from position (a) to position

Table 5 Relevant process properties

Straightening speed /(m min^{-1})	Pushing speed /(mm s^{-1})	Convex roller speed /(ral s^{-1})	Concave roller speed /(ral s^{-1})	Roller angle /(°)
30	300	6.76	7.78	25

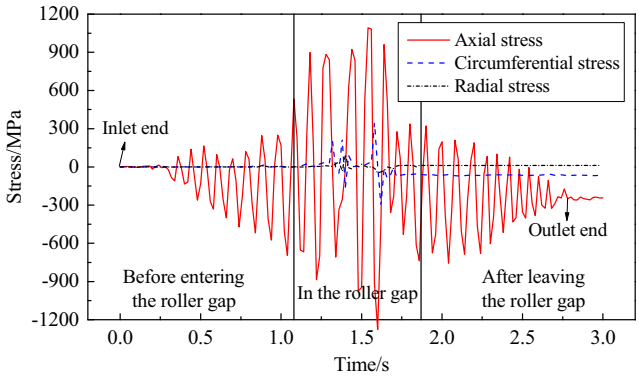

Fig. 13 Variation curves of stress with time on one node

(c), and after position (c) the compressive stress of the node B changes to tensile stress and increases gradually. When the section rotates 180 degrees to position (e), the axial stress of the node A and B reaches the maximum, which shows that the section is subjected to a single bending. As the section rotates from position (e) to position (g), the axial compressive stress of the node A decreases. When the section rotates 270 degrees and passes through the position (g), the compressive stress of the node A changes to tensile stress and increases gradually. Similarly, the axial tensile stress of the node B decreases

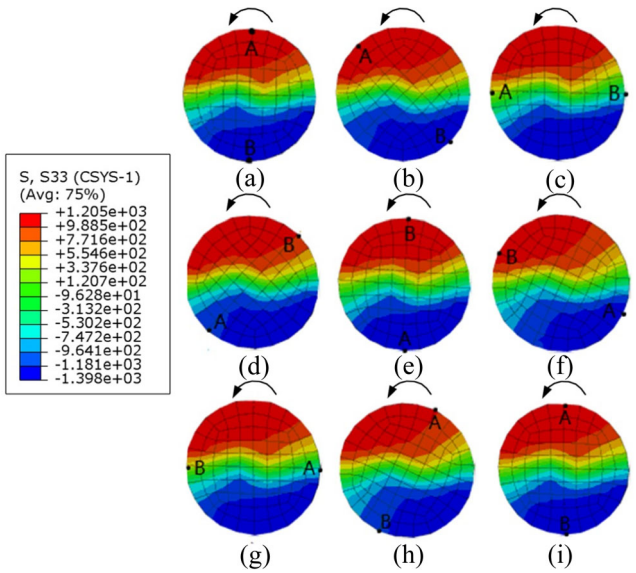

Fig. 14 Variation of axial stress of node A and node B on arbitrary cross section

gradually from position (e) to position (g), and after position (c) the tensile stress of the node B changes to compressive stress and increases gradually. When the section rotates to position (i), the axial stress of the node A and B reaches the maximum, which shows that the section is subjected to a single bending again.

Figure 15 shows the equivalent strain distribution of bar after straightening. It can be seen in Fig. 15 that the plastic strain of the bar decreases gradually from the surface to the center, and the center only occurs the elastic deformation. The maximum residual deflection of the bar along the x axis is 0.59 mm/m, the maximum residual deflection along the y axis is − 0.71 mm/m, and the maximum total residual deflection is 0.92 mm/m, a good straightening effect has been achieved.

Based on the above analysis, in the two-roller straightening process, the node on each section of the bar undergoes a cyclic tension-compression load, that is, each section undergoes reciprocating bending. It is proved an objective fact of realizing the purpose of straightening by reciprocating bending in the two-roller straightening process.

6 Conclusions

1. By analyzing the deformation path of the bar through the roller gap, the process of reciprocating bending is recognized macroscopically in the two-roller straightening process.
2. By means of graphical method and mathematical induction, it is proved that although the initial curvature of each section of bar is different, the difference of initial curvature is eliminated by reciprocating bending, and the mechanism of the two-roller straightening process is revealed.
3. The speed of curvature unification is determined mainly by the ratio of plastic modulus to elastic modulus. The greater the ratio of plastic modulus to elastic modulus is, the slower the speed of curvature uniformity is, and the more the bending time required, i.e., the more the number of spiral leads is.
4. The design of roller shape should be based on the design rule that the deformation degree of each micro-beam increases first and then decreases with the bending time. In the quantitative theory analysis, the residual curvatures of

Fig. 15 Equivalent strain distribution after straightening

5 micro-beams with different initial curvature after 4 times of bending are almost the same, and their value is close to zero.

5. In the two-roller straightening process, the stress of the bar is mainly determined by axial stress, and the value of axial stress changes alternately, which shows that the node is subjected to a cyclic tensile-compressive load and the section is subjected to reciprocating bending.

Funding information This project was funded and supported by the National Natural Science Foundation of China (51575473), Iron and Steel Research Foundation of Hebei province (E2016203209), Natural Science Foundation of Hebei Province (E2015203244 and E2016203266), and the Youth Talent Support Plan of Hebei Province in China.

References

1. Cui F (2007) Straightening theory and straightening machine. Metallurgical Industry Press, Beijing
2. Liu ZF, Wang YQ, Yan XC (2012)A new model for the plate leveling process based on curvature integration method. Int J Mech Sci 54(1): 213-224. doi: https://doi.org/10.1016/j.ijmecsci.2011.10.011
3. Yin J, Zhao J, Wang SY, Wan XS, Li YL (2014) Principle of multi-roller straightening process and quantitative resolutions of straightening strategies. J Iron Steel Res Int 21(9):823–829. https://doi.org/10.1016/S1006-706X(14)60148-5
4. Kaiser R, Stefenelli M, Hatzenbichler T, Antretter T, Hofmann M, Keckes J, Buchmayr B (2014) Experimental characterization and modelling of triaxial residual stresses in straightened railway rails. J Strain Anal Eng 50(3):190–198. https://doi.org/10.1177/0309324714560040
5. Zhao J, Song XK (2014) Control strategy of multi-point bending one-off straightening process for LSAW pipes. Int J Adv Manuf Tech 72(9–12):1615–1624. https://doi.org/10.1007/s00170-014-5776-9
6. Talukder NKD, Johnson W (1981) On the arrangement of rolls in cross-roll straighteners. Int J Mech Sci 23(4):213–220. https://doi.org/10.1016/0020-7403 (81)90046-1
7. Talukder NKD, Singh AN, Johnson W (1990) Cross-roll straighteners and their performance. J Mater Process Tech 21(1):101–109. https://doi.org/10.1016/0924-0136(90)90033-Q
8. Talukder NKD, Singh AN (1991) Mechanics of bar straightening, part 1: general analysis of straightening process. J Eng Ind 113(2): 224–227. https://doi.org/10.1115/1.2899682
9. Talukder NKD, Singh AN (1991) Mechanics of bar straightening, part 2: straightening in cross-roll straighteners. J Eng Ind 113(2): 228–232. https://doi.org/10.1115/1.2899683
10. Kawai KI, Satake M, Inoue Y, Sugita H (1995) Rotary forming for the straightening of tubing. J Mater Process Tech 48(1):135–141. https://doi.org/10.1016/0924-0136(94)01643-F
11. Li KY, Chen CK, Yang SC (1999) Profile determination of a tube-straightening roller by envelope theory. J Mater Process Tech 94(2–3):157–166. https://doi.org/10.1016/S0924-0136(99)00089-8
12. Wu BJ, Chan LC, Lee TC, Ao LW (2000) A study on the precision modeling of the bars produced in two cross-roll straightening. J Mater Process Tech 99(99):202–206. https://doi.org/10.1016/S0924-0136(99)00421-5
13. Huh H, Jin HH, Lee HW (2003) Optimization of a roller levelling process for Al7001T9 pipes with finite element analysis and Taguchi method. Int J Mach Tool Manu 43(4):345–350. https://doi.org/10.1016/S0890-6955(02)00269-9
14. Kuboki K, Huang H, Murata M, Yamaguchi Y, Kuroda K (2010) FEM analysis of tube straightener adopting implicit scheme. Steel Res Int 81(9):584–587. https://doi.org/10.1002/srin.201190002
15. Mutrux A, Berisha B, Hora P (2011) Prediction of cyclic softening in a medium carbon steel during cross roll straightening. J Mater Process Tech 211(8):1448–1456. https://doi.org/10.1016/j.jmatprotec.2011.03.019
16. Wang Y, Liu C, Ma LD, Huang Q (2012) Numerical simulation and application for process parameters of two-roll straightening. ICIC Express Letters 6(11):2781–2787
17. Wang Y, Liu C, Ma LD, Wang YF, Huang QX (2013) Analysis of interval between guides during two-roll straightening process. J Jilin Univ (Eng Tech) 03:677–681. https://doi.org/10.7946/jdxbgxb201303020
18. Moon C, Kim N (2013) Dimensional change in drawn wire product in the two cross-roll straightening process. T Korean Soc Mech Eng A 37(3):295–302. https://doi.org/10.3795/KSME-A.2013.37.3.295
19. Ma LF, Ma ZY, Jia WT, Lv YY, Jiang YP, Xu HJ, Liu PT (2015) Research and verification on neutral layer offset of bar in two-roll straightening process. Int J Adv Manuf Tech 79(9–12):1519–1529. https://doi.org/10.1007/s00170-015-6899-3
20. Jindřich P, Tomáš N, František Š (2016) Novel approach to computational simulation of cross roll straightening of bars. J Mater Process Tech 233:53–67. https://doi.org/10.1016/j.jmatprotec.2016.02.004
21. Zhang ZQ, Yan YH, Yang HL (2013) The straightening curvature-radius model for the thin-walled tube and it's validation. J Mech Eng 21:160–167. https://doi.org/10.3901/JME.2013.21.160
22. Zhang ZQ (2016) Prediction of maximum section flattening of thin-walled circular steel tube in continuous rotary straightening process. J Iron Steel Res Int 23(8):745–755. https://doi.org/10.1016/S1006-706X(16)30116-9
23. Zhang ZQ, Yan YH, Yang HL (2016) A simplified model of maximum cross-section flattening in continuous rotary straightening process of thin-walled circular steel tubes. J Mater Process Tech 238:305–314. https://doi.org/10.1016/j.jmatprotec.2016.07.034
24. Wang YQ, Liu ZF, Ou HG, Luo YX, Yan XC (2016) Curvature and residual stress analysis in rotational leveling of bars. J Iron Steel Res Int 07:669–676. https://doi.org/10.1016/S1006-706X(16)30104-2
25. Yu GC, Zhao J, Zhai RX, Ma R, Wang CG (2016) Theoretical analysis and experimental investigations on the symmetrical three-roller setting round process. Int J Adv Manuf Tech. https://doi.org/10.1007/s00170-016-9610-4
26. Zhao J, Yu GC, Ma R (2016) A mechanical model of symmetrical three-roller setting round process: the static bending stage. J Mater Process Tech 231:501–512. https://doi.org/10.1016/j.jmatprotec.2016.01.002
27. Zhao J, Yin J, Ma R, Ma LX (2011) Springback equation of small curvature plane bending. Sci China Technol Sci 54(9):2386–2396. https://doi.org/10.1007/s11431-011-4447-4